Available online at www.sciencedirect.com

ScienceDirect

Advances in Space Research 65 (2020) 1279–1295

ADVANCES IN SPACE RESEARCH (a COSPAR publication)

www.elsevier.com/locate/asr

PD and PD^{β} based sliding mode control algorithms with modified reaching law for satellite attitude maneuver

Debajyoti Chakrabarti [a], N. Selvaganesan [b,*]

[a] Control Dynamics & Analysis Division II(CDAD-II), Control Dynamics & Simulation Group(CDSG), U. R. Rao Satellite Centre Bangalore-560017, India
[b] Department of Avionics, Indian Institute of Space Science and Technology (IIST), Department of Space (DOS), Govt. of India, Thiruvananthapuram 695 547, India

Received 17 July 2019; received in revised form 23 October 2019; accepted 5 November 2019
Available online 20 November 2019

Abstract

Attitude Determination and Control System of a satellite, can be regarded as one of the major subsystems of satellite design. The dynamics and kinematics of the satellite are important to design a controller. In this paper, the nonlinear mathematical model of a satellite is formulated using quaternions. Further, reaction wheel assembly is chosen as an actuator which provides the necessary torque to control the satellite attitude. To stabilize the satellite at desired attitude and angular velocity, PD and PD^{β} based sliding mode controllers with modified reaching law are proposed. An optimization problem is presented to tune the parameters of the proposed controllers. Numerical simulation is carried out for the satellite system with the tuned controllers at various operating conditions such as (i) without disturbance, (ii) with disturbance and (iii) robustness towards parameter uncertainty. The results of the proposed controllers are compared with conventional PD and PD^{β} sliding mode controllers.

Keywords: Satellite system; Reaction wheel; Fractional order sliding mode control; Power rate type reaching law

1. Introduction

The attitude of a satellite is defined as the orientation of the satellite with respect to some inertial frame of reference or with respect to some coordinate system in space. The Attitude Determination and Control System (ADCS) is one of the most important subsystems of a spacecraft, which consists of two processes namely attitude determination and attitude control Sidi (1997). The ADCS determines the current orientation of the spacecraft with respect to fixed inertial reference frame by using external references and sensors. Based on the feedback information, the attitude control system provides the required torque to the reaction wheel assembly which is considered as an actuator. The performance of the satellite is effected due to disturbances caused by solar radiation pressure, aerodynamic drag due to earth's atmosphere, interaction with earth's magnetic field and gravity gradient torque.

The mathematical modelling of the spacecraft based on various methods of attitude representation and the modern spacecraft control techniques are presented in Sidi (1997) and Wertz (2012). The attitude of the satellite is defined using quaternion, Euler angle and direction cosine matrix. Quaternion concepts, quaternion algebra, geometry and rotation using quaternions have been well established in Kuipers et al. (1999). The applications and working of different actuators like reaction wheel, reaction thrusters, momentum wheel and magneto torquer in satellite attitude control is given in Bryson (2015) and Vadali (1986). The dynamics of the reaction wheel is described in Blanke and Larsen (2010),Froelich and Papapoff (1959) and the

* Corresponding author.
E-mail address: n_selvag@iist.ac.in (N. Selvaganesan).

https://doi.org/10.1016/j.asr.2019.11.005
0273-1177/

concepts of momentum based actuators for satellite attitude control is discussed in Siahpush and Gleave (1988).

The basic theory and principles of sliding mode control design are explained in Shtessel et al. (2014) and Utkin (1993). Description of sliding mode control with accurate assessment on chattering is given in Young et al. (1996). In Crassidis and Markley (1996), a sliding mode controller is proposed using modified Rodriguez parameters. Sliding mode control (SMC) law for attitude control of rigid satellite is proposed in Wu et al. (2009) followed by modification in control law by introducing disturbance observer to remove chattering effect and also to improve the control effort. Sliding mode controller with fast reaching time and less chattering is suggested in Ibrahim et al. (2012) for end-to-end maneuvers with external disturbances on quaternion based satellite model having angular velocity constraints. A robust sliding mode controller for spacecraft attitude control problem is proposed in Chen and Lo (1993) and the spacecraft attitude is represented using Gibbs vector of Rodriguez parameter. The stability of the designed controller is analysed with direct method of Lyapunov stability. In Liu and Wang (2012) and Bandyopadhyay et al. (2013), the design and analysis of conventional and different advanced sliding mode controllers for different mechanical systems have been described. A sliding mode control for the attitude control of a communication satellite has been proposed using Euler angle representation in Abdulhamitbilal and Jafarov (2012). The large angle maneuver problem of a spacecraft using the concept of variable structure control theory is treated in Vadali (1986). In Abdulhamitbilal and Jafarov (2008), the attitude control of a geosynchronous communication satellite with thrust jets by using SMC technique is presented. The attitude tracking control problem of a spacecraft with external disturbances and inertia uncertainties are addressed in Lu et al. (2012).

In Mirhassani et al. (2013), the attitude and speed control of geostationary satellites using *PD* and SMC are presented. A variable structure control with improved pseudoinverse is developed in Yu et al. (2011) based on the error quaternion satellite model, which overcomes the non uniqueness of pseudoinverse matrix in addition to meet the required specifications. The attitude control of a spacecraft using eigen axis maneuver in presence of parameter uncertainty and external disturbances has been proposed in Chen et al. (2013). In Abdulhamitbilal and Jafarov (2006), the comparison of performances of a linear control and SMC for attitude control of the spacecraft with reaction wheels are presented.

In recent years, linear control laws have been incorporated in conventional sliding mode design for better performance. In Ghazali et al. (2011), the position tracking performance of an electro-hydraulic servo system having a friction nonlinearity using SMC with Proportional Integral Derivative (*PID*) sliding surface is presented and the performance is compared with conventional *PID* controller. In Ahmed et al. (2012), sliding mode control with *PID* sliding surface is proposed for a coupled tank system. Sliding mode controller having *PID* sliding surface for speed control of electromechanical plant is discussed in Eker (2006). The above-mentioned controller with hyperbolic function is used to remove the chattering effect. In Qi and Wang (2016), sliding mode controller is suggested for active queue management using *PID* sliding surface which changes to *PD* sliding surface when the instantaneous queue length error is greater than command input. In Song et al. (2017), *PD* sliding surface is used for sliding mode control of high speed railway pantograph catenary contact force under strong stochastic wind field. *PD* in combination with SMC is used in Acob et al. (2013), Jin et al. (2018), Ouyang et al. (2014) to incorporate the advantages of both PD and SMC in the hybrid control structure. In Tang et al. (2017), non linear PD control is combined with SMC for trajectory tracking control of a 3-DOF planar robotic manipulator.

Various methods have been suggested in literature for alleviation of chattering. One such method to remove chattering is boundary layer control, in which piecewise linear or smooth approximation of the switching element in a boundary layer of the sliding manifold is carried out in Utkin (1993), Young et al. (1996). However disadvantage with boundary layer control is that it causes loss of ideal sliding motion which effects directly on the robustness property of the system. Observer based SMC is proposed for removal of chattering in Young et al. (1996), Wu et al. (2009). Reaching law based control method is another way to alleviate chattering and also to control the reaching time as discussed in Gao and Hung (1993), Jerouane et al. (2004). Power rate type reaching law is one among them where both reaching time improvement and chattering removal can be adressed. A modification of power rate type reaching law, called as Power Rate Exponential Reaching Law (PRERL) is proposed in Devika and Thomas (2017) for further improvement in performance compared to normal power rate type reaching law.

Fractional calculus generalizes integer order calculus to any order Monje et al. (2010). In control engineering, fractional calculus finds applications in either system modelling or controller design. The compact irrational form transfer function structure of fractional order controller can meet stringent loop shaping requirements. Literature Monje et al. (2010)–Xue et al. (2007) shows that being the superclass of their integer counterparts, fractional controllers always perform better, e.g. fractional *PI* is better than integer *PI*. Fractional order calculus and its definitions, properties, computations, time domain analysis and filter approximation techniques have been explained in Xue et al. (2007). In Xinsheng and Huaqiang (2015), a fractional order controller of the structure $[PD]^{\beta}$ (β being the fractional order) is designed for attitude control of a satellite with pulse width pulse frquency modulator as thruster. For attitude stabilization of low earth orbit satellite, fractional controller of the structure $PD^{(1+\beta)}$ is suggested in Kailil et al. (2004b) and the performance of the controller is compared with Linear Quadratic Regulator. A Fractional Order Sliding Mode Control (FOSMC) for pico satellite using reduced quaternion model in presence of gravity gradient disturbance torque is proposed in Valério (2012) and Liwei and Shenmin (2013), where sliding surfaces are fractional. FOSMC is proposed with different sliding surfaces using modified Rodriguez parameter in Tianyi et al. (2015). A fractional regulator for spacecraft attitude stabilization is introduced in Kailil et al. (2004a) and a comparative study between fractional and optimal control law has been established. A FOSMC with two subsliding manifolds is presented in Kang et al. (2017) for the deployment of tethered space systems with external disturbances and unmodeled dynamics. In Tepljakov et al. (2011), all the major modules comprising the FOMCON toolbox, the analysis of fractional order systems, identification, controller design, tuning and optimization are presented. Fractional sliding surface of the form PD^{β} is introduced in Lazarević (2012) for position control of 3 DOF robotic system driven by DC motors. In Rahimian and Tavazoei (2013), optimal tuning method for fractional controllers is proposed. Stability of fractional order (FO) systems is investigated in Sara et al. (2017) in the sense of Lyapunov theory. In Ahmed et al. (2018), fractional-order (FO) with nonsingular fast terminal sliding mode control (NFTSM) is proposed for a robotic exoskeleton under parametric uncertainties and external disturbances, to track a given trajectory along with absence of singularity and chattering, also ensuring fast finite time convergence, followed by time delayed estimation of the disturbances and uncertainties making the controller model independent. Model free controller is proposed in Ahmed et al. (2019a), to control n-degree of freedom robotic manipulator in presence of disturbance and backlash hysterisis. Time delay part of the proposed controller takes care of the unknown dynamics of the manipulator whereas adaptive terminal sliding part of the controller handles robustness and finite time convergence issues. The superiority of the proposed controller is established by comparing the results with existing adaptive fractional order terminal sliding mode control under backlash hysteresis. Combined advantages of fractional-order and non-singular fast terminal sliding mode control is demonstrated in Ahmed et al. (2019b), for control of a lower-limb exoskeleton under disturbance and uncertanties. The proposed control law not only shows good tracking performance, but also ensures fast and finite time convergence, non-singularity and significant reduction of chattering effect.

From the above works, it is evident that PD-SMC and PD^{β}-SMC laws are good options for satellite attitude control as they incorporate advantages of both linear and SMC law. But similar to conventional SMC, PD-SMC and PD^{β}-SMC also suffer from the chattering problem. The usage of saturation/hyperbolic function instead of signum function in the control law to remove chattering (boundary layer control) results in the reduction of robustness towards disturbance. Therefore, it is necessary to remove chattering in case of PD-SMC and PD^{β}-SMC, at the same time maintain robustness property. This motivates us to introduce PD and PD^{β} based sliding mode control with modified reaching law for ADCS.

The contribution of the paper is summarized as follows:

(i) PD-SMC and PD^{β}-SMC with modified reaching law are proposed to control the satellite attitude.
(ii) The expression for reaching time, convergence and stability proof in terms of Lyapunov are discussed for the proposed controllers.
(iii) The numerical simulation is carried out for the proposed PD-SMC and PD^{β}-SMC with modified reaching law under disturbance rejection and robustness against parameter variation. The obtained results are compared with conventional PD-SMC and PD^{β}-SMC.

This paper is organised as follows. In Section 2, the modelling of the spacecraft and actuator are described. Generalized block diagram representation and various non linear controllers namely PD-SMC, PD^{β}-SMC, Modified PD-SMC and Modified PD^{β}-SMC are discussed in Section 3. The detailed simulation and performance comparision for various controllers under different cases are presented in Section 4. Section 5 presents the conclusion and future research directions.

2. Mathematical modelling of satellite

Mathematical modelling of satellite consists of two parts: Dynamics and Kinematics Wie (1998).

2.1. Modelling of dynamics

Satellite attitude dynamics is modelled using *Euler-moment equation* described in Sidi (1997), Wertz (2012) and it is given as:

$$J\dot{\omega} + \omega \times (J\omega + h_w) + \dot{h}_w = T_e + T_d \tag{1}$$

where $J \in \mathbb{R}^{3\times 3}$ is the moment of inertia matrix for the satellite, $\omega = [\omega_1, \omega_2, \omega_3]^T$ is the angular velocity of body frame of the satellite with respect to inertial frame of reference, $h_w = [h_{w1}, h_{w2}, h_{w3}]^T$ is the angular momentum vector of reaction wheel assembly, T_d is the disturbance torque acting on the satellite and T_e is the external control torque acting on satellite. The skew symmetric matrix $\omega\times$ is given by,

$$\omega\times = \begin{bmatrix} 0 & -\omega_3 & \omega_2 \\ \omega_3 & 0 & -\omega_1 \\ -\omega_2 & \omega_1 & 0 \end{bmatrix} \tag{2}$$

In this paper, satellite model consists of 3 reaction wheels aligned along satellite body coordinates and this reaction wheel assembly is used as an actuator, which provides the necessary control torque on the satellite. Since $T_e = 0, T_c = -\dot{h}_w$ is the only control torque (internal) acting on the satellite. Hence modified attitude dynamics of satellite with control torque applied from reaction wheel assembly is as follows:

$$J\dot{\omega} + \omega \times (J\omega + h_w) = T_c + T_d \tag{3}$$

2.2. Modelling of kinematics

Among various existing techniques to represent the kinematic equation for satellite, quaternion method of representation is followed throughout this work. The kinematic equation describing the time evaluation of satellite attitude described in Kuipers et al. (1999), Bekir (2007) is given as:

$$\begin{bmatrix} \dot{q} \\ \dot{q}_4 \end{bmatrix} = \frac{1}{2}\begin{bmatrix} q_4\omega - \omega \times q \\ -\omega^T q \end{bmatrix} \tag{4}$$

where $q = [q_1, q_2, q_3]^T$ is the vector part of the quaternion and q_4 is the scalar part of the quaternion.

2.3. Actuator dynamics

Consider T_w be the torque provided from stator to the rotor of reaction wheel, then dynamic relation between T_w and T_c is given by the following equation Blanke and Larsen (2010),

$$\tau_w \ddot{h}_w = -\dot{h}_w + T_w \tag{5}$$

$$T_c = -\dot{h}_w \tag{6}$$

$$h_w(t) = \int_0^t \dot{h}_w(\tau)d\tau + h_w(0) \tag{7}$$

where τ_w is the time constant of the reaction wheel.

From (5), (6), the relation between T_c and T_w in Laplace domain is given by,

$$T_c = -\frac{1}{\tau_w s + 1} T_w \tag{8}$$

2.4. Combined nonlinear model

Combining (3)–(6) the overall nonlinear model for the angular motion of the satellite is obtained as following,

$$\frac{d}{dt}\begin{bmatrix} \omega \\ q \\ q_4 \\ h_w \\ \dot{h}_w \end{bmatrix} = \begin{bmatrix} J^{-1}(-\omega \times (J\omega + h_w) + T_c + T_d) \\ -\frac{1}{2}\omega \times q + \frac{1}{2}q_4 I_{3\times3}\omega \\ -\frac{1}{2}\omega^T q \\ -T_c \\ -\frac{1}{\tau_w}\dot{h}_w + \frac{1}{\tau_w}T_w \end{bmatrix} \tag{9}$$

3. Controller design

3.1. Generalized block diagram representation

The proposed generalized structure of the satellite attitude control system, is shown in Fig. 1. It consists of (i) satellite model and (ii) sliding mode based controller. Satellite model comprises of reaction wheel dynamics, satellite dynamics and kinematics block. Sliding mode controller contains sliding surface block and control algorithm block. In Fig. 1, $T_{control}$ (T_w) is the torque acting on the reaction wheel rotor. T_c is the torque applied on the satellite from the reaction wheel assembly and h_w denotes the angular momentum of reaction wheel assembly. Angular velocity and quaternion initial conditions are provided to satellite dynamics block and kinematics block using $\omega_{initial}$ and $q_{initial}$ blocks respectively.

Let q_s and q_r be the measured and reference satellite quaternions. The error quaternion (q_{er}) is a 4×1 vector defined as below Sidi (1997):

$$q_{er} = q_s^{-1} \otimes q_r = \begin{bmatrix} q_{s4} & q_{s1} & q_{s2} & q_{s3} \\ -q_{s1} & q_{s4} & q_{s3} & -q_{s2} \\ -q_{s2} & -q_{s3} & q_{s4} & q_{s1} \\ -q_{s3} & q_{s2} & -q_{s1} & q_{s4} \end{bmatrix}\begin{bmatrix} q_{r4} \\ q_{r1} \\ q_{r2} \\ q_{r3} \end{bmatrix} = \begin{bmatrix} q_{e1} \\ q_{e2} \\ q_{e3} \\ q_{e4} \end{bmatrix} \tag{10}$$

where $\otimes$ implies quaternion multiplication. Vector part of error quaternion is denoted by q_e which equals to $[q_{e1}, q_{e2}, q_{e3}]^T$. Angular velocity error (ω_e) is defined as,

$$\omega_e = \omega_r - \omega_s = \begin{bmatrix} \omega_{e1} \\ \omega_{e2} \\ \omega_{e3} \end{bmatrix} \tag{11}$$

where $\omega_r = \begin{bmatrix} \omega_{rx} \\ \omega_{ry} \\ \omega_{rz} \end{bmatrix}$ is the reference angular velocity and $\omega_s = \begin{bmatrix} \omega_{sx} \\ \omega_{sy} \\ \omega_{sz} \end{bmatrix}$ is the satellite angular velocity.

3.2. Nonlinear controller design

The objective of the control law design is to attain desired quaternions and angular velocity (q_e, ω_e to zero). This section presents *PD* sliding mode control (*PD*-SMC), PD^β sliding mode control (PD^β-SMC), *PD* sliding mode control with modified reaching law and PD^β sliding mode control (PD^β-SMC) with modified reaching law to control the attitude of the satellite.

3.2.1. PD Sliding Mode Controller (PD-SMC)

Design of *PD*-SMC consists of two phases namely (i) design of sliding surface, (ii) design of control law that stabilizes the system. Choice of sliding surface (S) is followed from *PD* control law for 3 axis satellite attitude control Sidi (1997),Wertz (2012):

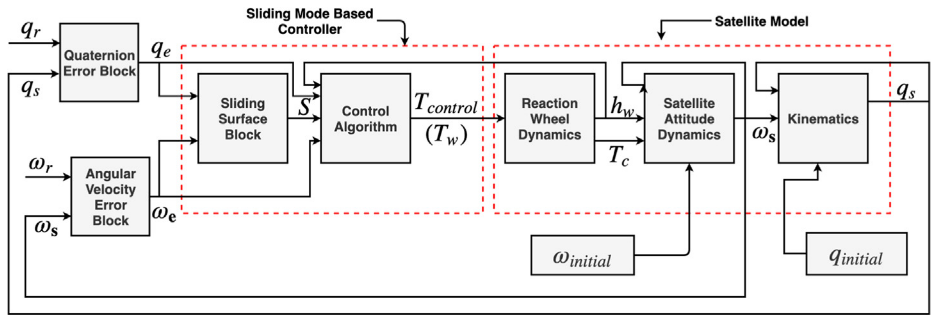

Fig. 1. Block diagram of satellite attitude control system.

$$S = 2K_P q_e + K_D\omega_e \tag{12}$$

where K_P and K_D are the parameters of PD controller and S consists of 3 components namely $[S_x, S_y, S_z]^T$.

PD-SMC Control law expression ($T_{control}$) has two parts to be designed namely: (i) Equivalent control law (u_{eq}) and (ii) Discontinuous Control Law ($u_{discont}$).

$$T_{control} = u_{eq} + u_{discont} \tag{13}$$

For design of u_{eq}, (12) is differentiated and equated to zero which is as follows:

$$\dot{S} = 2K_P\dot{q}_e + K_D\dot{\omega}_e = 0 \tag{14}$$

Based on (4), $\dot{q}_{er}$ is obtained:

$$\dot{q}_{er} = \begin{bmatrix} \dot{q}_e \\ \dot{q}_{e4} \end{bmatrix} = \frac{1}{2}\begin{bmatrix} q_{e4}\omega_e - \omega_e \times q_e \\ -\omega_e^T q_e \end{bmatrix} \tag{15}$$

From (15), relation between $\dot{q}_e$ and ω_e can be written as,

$$\dot{q}_e = \frac{1}{2}(q_{e4}\omega_e - \omega_e \times q_e) = \frac{1}{2}\begin{bmatrix} q_{e4} & -q_{e3} & q_{e2} \\ q_{e3} & q_{e4} & -q_{e1} \\ -q_{e2} & q_{e1} & q_{e4} \end{bmatrix}\omega_e = \frac{1}{2}Q_e\omega_e \tag{16}$$

Substituting (16) and (3) in (14), u_{eq} is obtained as,

$$u_{eq} = \omega_e \times (J\omega_e + h_w) - \frac{K_P}{K_D}JQ_e\omega_e \tag{17}$$

The discontinuous part of control law is chosen as Edwards and Spurgeon (1998),

$$u_{discont} = -Ksgn(S) \tag{18}$$

where K represents gain of the nonlinear control law.

Using (17) and (18) in (13), expression for $T_{control}$ is given as,

$$T_{control} = \omega_e \times (J\omega_e + h_w) - \frac{K_P}{K_D}JQ_e\omega_e - Ksgn(S) \tag{19}$$

where $sgn(S) = [sgn(S_x), sgn(S_y), sgn(S_z)]^T$; 'sgn' denotes signum function.

The proofs for Finite Time Convergence (FTC), stability condition and expression for reaching time of the PD-SMC control law are obtained and given in Appendix (A.1)–(A.7) and (A.8)–(A.10).

3.2.2. PD^β Sliding Mode Controller (PD^β-SMC)

The design of PD^β-SMC for satellite system is similar to integer order SMC design and consists of two stages namely (i) design of sliding surface and (ii) design of control law which makes system states attracted to the surface. The sliding variable of PD^β-SMC is chosen as below Kailil et al. (2004b), Lazarević (2012):

$$S = 2K_P q_e + K_D D^\beta\omega_e \tag{20}$$

where K_P and K_D are the parameters of PD^β controller and D^β denotes *Caputo fractional derivative operator* of order β Monje et al. (2010),

$${}_aD_t^\beta f(t) = \begin{cases} \frac{1}{\Gamma(m-\beta)}\int_a^t \frac{f^{(m)}(\tau)}{(t-\tau)^{\beta-m+1}}d\tau & m-1<\beta<m \\ \frac{d^m}{dt^m}f(t) & \beta = m \end{cases} \tag{21}$$

where m is the smallest integer bigger than β, $\Gamma(x) = \int_0^\infty e^{-x}x^{n-1}dx$ is the Gamma function.

Like PD-SMC design, the expression for u_{eq} is obtained by differentiating (20) with respect to time and equating it zero.

$$\dot{S} = 2K_P\dot{q}_e + K_D D^\beta\dot{\omega}_e = 0 \tag{22}$$

Using (16) and (3) in (22), expression for u_{eq} is derived as,

$$u_{eq} = \omega_e \times (J\omega_e + h_w) - \frac{K_P}{K_D}JD^{-\beta}Q_e\omega_e \tag{23}$$

The discontinuous part of control law is selected and as follows,

$$u_{discont} = -K_f D^{-\beta}sgn(S) \tag{24}$$

where K_f is the gain of discontinuous control law.

Hence from (13), (23) and (24) the net control torque is derived.

$$T_{control} = \omega_e \times (J\omega_e + h_w) - \frac{K_P}{K_D}JD^{-\beta}Q_e\omega_e - K_f D^{-\beta}sgn(S) \tag{25}$$

The proofs for FTC towards sliding surface, stability and reaching time expression of PD^β-SMC are provided in Appendix (A.11)–(A.23) and (A.24)–(A.26).

3.2.3. PD-SMC with modified reaching law

For design of PD-SMC with modified reaching law, sliding surface is chosen same as in (12) and modified reaching law Gao and Hung (1993), Jerouane et al. (2004), Devika and Thomas (2017) is selected as,

$$\dot{S} = -K_m|S|^{\alpha} sgn(S) \tag{26}$$

where K_m is the gain of the modified reaching law, $0 < \alpha < 1$ and

$|S|^{\alpha} = diag[|S_x|^{\alpha}, |S_y|^{\alpha}, |S_z|^{\alpha}]$ ('diag' means diagonal of a diagonal matrix).

Using (3) and (16) in the comparison of the time derivative of (12) with (26), the expression of the net control torque developed for PD-SMC with modified reaching law is given as below:

$$T_{control} = \omega_e \times (J\omega_e + h_w) - \frac{K_P}{K_D} JQ_e\omega_e - \frac{K_m}{K_D} J|S|^{\alpha} sgn(S) \tag{27}$$

The proofs for FTC towards sliding surface, stability and reaching time expression of PD-SMC with modified reaching law are provided in Appendix (A.27)-(A.30) and (A.31) and (A.32).

3.2.4. PD^{β}-SMC with modified reaching law

In this section, PD^{β}-SMC law is designed with modified reaching law. The sliding surface is selected same as in (20) and the modified reaching law is similar to the reaching law proposed in (26),

$$\dot{S} = -K_{mf}|S|^{\alpha} sgn(S) \tag{28}$$

where K_{mf} is the gain of the modified reaching law.

For design of control law, derivative of S (from (20)) is compared to (28) and the expression of $T_{control}$ is obtained by using (3), (16) and it is given as,

$$T_{control} = \omega_e \times (J\omega_e + h_w) - \frac{K_P}{K_D} JD^{-\beta}Q_e\omega_e - \frac{K_{mf}}{K_D} JD^{-\beta}(|S|^{\alpha} sgn(S)) \tag{29}$$

Proof of FTC, stability and reaching time calculation for PD^{β}-SMC with modified reaching law are presented in Appendix (A.33)–(A.36) and (A.37) and (A.38).

3.3. Tuning of controller parameters

The parameters of the various non linear control laws presented in Section 3.2 are tuned using generalized optimization procedure. The given optimization problem is unconstrained and the objective function is the combination of performance indices namely, control effort, Integral Time Absolute Error (ITAE) and Integral Square Error (ISE). It is formulated as below:

$$\underset{x}{\text{Minimize}}\ C_0\sum_{i=1}^{3}\int_t t|\omega_{ei}(x,t)|dt + C_1\sum_{i=1}^{3}\int_t T^2_{control,i}(x,t)dt + C_2\sum_{i=1}^{3}\int_t \omega^2_{ei}(x,t)dt + C_3\sum_{i=1}^{3}\int_t t|q_{ei}(x,t)|dt \tag{30}$$

where $i = 1, \cdots, 3$ represents 3 axes of satellite body coordinate frame. The coefficients C_0, C_1, C_2, C_3 are the weights of respective performance indices and to be chosen depending on the importance given to the respective performance indices, such that $\sum_{j=0}^{3} C_j = 1$.

As ω_s is the main variable to be controlled, both ISE and ITAE performance indices are considered with respect to ω_e to control both transient and steady state responses. For q_e, only steady state performance index (ITAE) is chosen considering that there is no large variation during transient state of q_e. The energy consumption by various subsystems of satellite is another crucial factor to be optimized. Hence, control effort performance index is chosen to minimize the energy consumption of satellite ADCS. Such combination is selected due to (i) control effort minimization donot ensure transient or steady state improvement and (ii) ISE or ITAE does not directly help in minimizing the control effort.

Depending on the control law, structure of x will vary. PD-SMC control law has 3 parameters to be tuned namely, $x = [K_P, K_D, K]$ and PD^{β}-SMC has 4 parameters to be tuned namely, $x = [K_P, K_D, K_f, \beta]$. The control algorithms with modified reaching law namely, PD-SMC with modified Reaching Law and PD^{β}-SMC with modified Reaching Law have 4 (K_P, K_D, K_m, α) and 5 $(K_P, K_D, K_{mf}, \beta, \alpha)$ parameters to be tuned respectively. The parameters of the various controllers are tuned using the given optimization procedure.

4. Simulation results

The simulation is performed with the designed controllers namely, PD-SMC, PD^{β}-SMC, PD-SMC with modified law and PD^{β}-SMC with modified reaching law

Table 1
Parameters of the satellite.

Parameters	Value
Initial Quaternion	[0.5 0.5 0.5 0.5]
Initial Angular Velocity	[0.02–0.07 0.05] rad/s
Desired Quaternion	[0 0 0 1]
Desired Angular Velocity	[0 0 0] rad/s
Inertia Matrix of the Satellite	$diag[50, 75, 100]$ Kg m^2
Inertia Matrix of the Reaction Wheel	$0.7259 \times 10^{-4} I_{3\times3}$ Kg m^2
Maximum Torque of the Reaction wheel	1 N m
Time Constant of the Reaction Wheel	100 ms

for the satellite attitude control under various conditions. The values of the satellite system parameters are listed in the Table 1.

4.1. Optimization of non linear controller parameters

Optimization problem formulated in Section 3.3 has 4 coefficients and are selected as, $C_x = [0.31, 0.15, 0.18, 0.36]^T$ such that ITAE of q_e and ω_e are given the most and second most preferences respectively to ensure their convergence to zero, which is the basic requirement of attitude control problem. Significant weightage is given to ISE of ω_e to reduce transient oscillation in angular velocity. Although remaining weightage is given to control effort, but it is ensured that weightage is significant compared to other coefficients.

Matlab optimization tool fminsearch has been used to design parameters of each controller. This utilizes Nelder-Mead simplex algorithm for simulation. After successive iterations/trials, the band of each controller is chosen as given in Table 2. For simulation purpose, 500 iterations are carried out with each controller to obtain unique optimization solution within the chosen band of parameters. To ensure the unique and global optimal solution, a random initial guess for the parameters are considered at every iteration. Hence the controller parameters which are presented for different cases are unique and the given optimization problem is not trapped into local minimum problem. Optimized gain values of each controller are listed in Table 3.

4.2. Closed loop simulation

Each of the controllers are simulated in the closed loop as shown in Fig. 1. Simulation is carried out for 200 s and responses for each controller under different conditions are given below.

4.2.1. Simulation results for PD-SMC

4.2.1.1. Case 1: Without disturbance. The simulation results of satellite attitude control problem with *PD*-SMC in the absence of disturbance are shown in Figs. 2 and 3. From Fig. 2, it is observed that the satellite settles to the desired quaternion and angular velocity within 24.87 s and the required control torque switching between ± 1 Nm, is presented in Fig. 3. Also chattering effect is visible in control torque response.

4.2.1.2. Case 2: With saturation function. To avoid the chattering effect, the signum function in the *PD*-SMC control signal is replaced with saturation function and the corresponding results are shown in Figs. 4 and 5. This leads to increase in the settling time to 25.15 s which is visible in Fig. 4.

4.2.1.3. Case 3: With disturbance. To verify the disturbance rejection capability of *PD*-SMC, a random disturbance (uniform distribution) is introduced to the system during 60th sec to 120th sec and the corresponding angular velocity and quaternion responses are shown in Fig. 6. The disturbance rejection property of the system is also verified for the case when signum function is replaced with saturation function shown in Fig. 8. It is observed that the effect of disturbance is negligible in the angular velocity and quaternion responses i.e. *PD*-SMC has shown good disturbance rejection capability. Corresponding control torque and sliding variable responses are shown in Figs. 7 and 9.

4.2.1.4. Case 4: With inertia matrix perturbation. To check the robustness of *PD*-SMC, perturbation is introduced to the inertia matrix of the satellite system. The simulation is performed with 40% and 60% perturbations in the inertia matrix at 120th sec. Since no change in response is observed with respect to case 1, corresponding responses are not included.

4.2.2. Simulation results for PD^{β}-SMC

4.2.2.1. Case 1: Without disturbance. The PD^{β}-SMC for satellite attitude control system is simulated without introducing disturbance. Figs. 10 and 11 show the angular velocity and quaternion response of PD^{β}-SMC controller. From Fig. 10, it is found that the satellite achieves the desired quaternion and angular velocity with settling time of 29.53 s and the required control torque response is presented in Fig. 11, switching between ± 1 Nm. Also chattering effect appears in control torque response.

4.2.2.2. Case 2: With saturation function. The signum function is used to avoid the chattering effect. The angular velocity and quaternion responses in case of PD^{β}-SMC are shown in Figs. 12 and 13 respectively. This clearly indicates that angular velocity response settles at 23.78 s.

4.2.2.3. Case 3: With disturbance. To show the capability of disturbance rejection, a random disturbance is given to

Table 2
Optimization band for different controllers.

Controller Name	Range of Parameters			
	K_P	K_D	β	Gain (K or K_m or K_f or K_{mf})
PD-SMC	[0,10]	[0,20]	–	[0,2.5]
PD-SMC with modified reaching law	[0,10]	[0,20]	–	[0,2.5]
PD^{β}-SMC	[0,10]	[0,20]	[0.5,1]	[0.5,2.5]
PD^{β}-SMC with modified reaching law	[0,10]	[1,20]	[0.5,1]	[0.5,2.5]

Table 3
Optimization result.

Controller Name	Parameters of Controller			
	K_P	K_D	β	Gain (K or K_m or K_f or K_{mf})
PD-SMC	2.3997	12.452	—	0.72617
PD-SMC with modified reaching law	2.53382	10.3046	—	0.21542
PD^{β}-SMC	6.8786	9.3969	0.2587	2.3646
PD^{β}-SMC with modified reaching law	3.6797	34.0124	0.1065	0.7

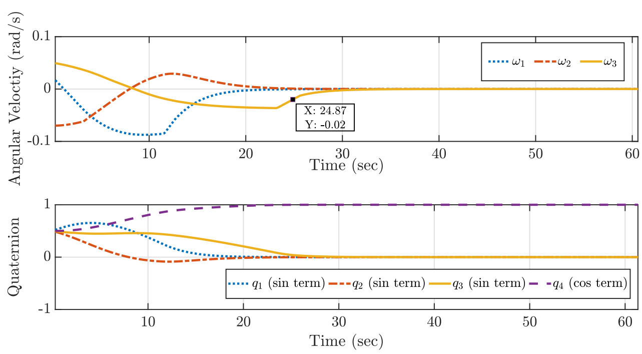

Fig. 2. Angular velocity and quaternion responses without saturation.

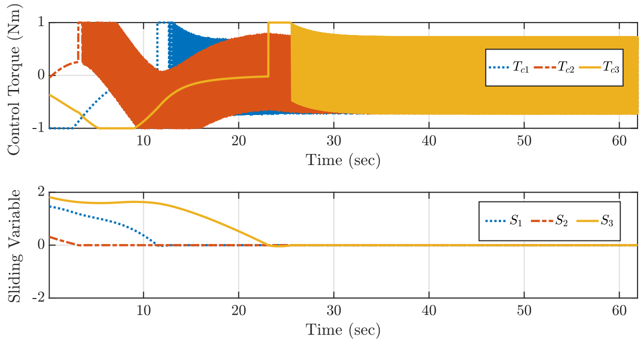

Fig. 3. Control torque and sliding variable responses without saturation.

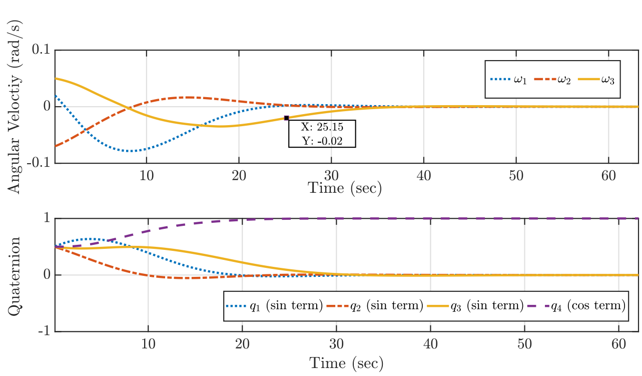

Fig. 4. Angular velocity and quaternion responses with saturation function.

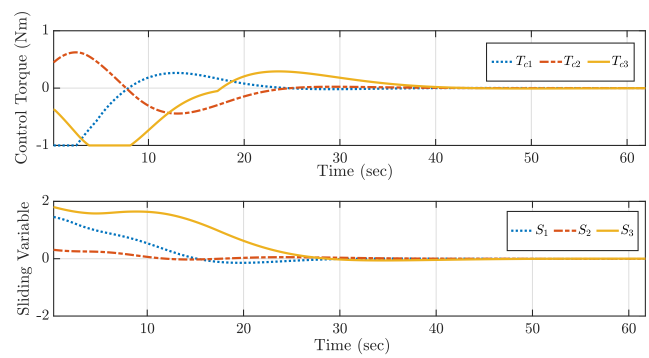

Fig. 5. Control torque and sliding variable responses with saturation function.

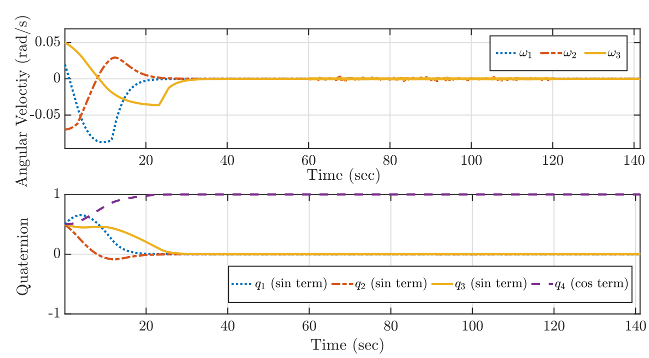

Fig. 6. Angular velocity and quaternion responses under disturbance.

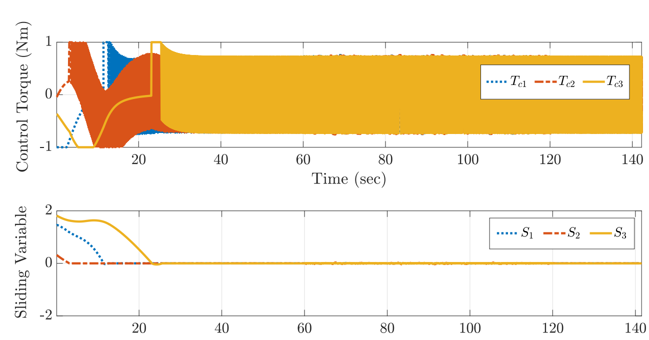

Fig. 7. Control torque and sliding variable responses under disturbance.

the system during 60th sec to 120th sec and the corresponding angular velocity and quaternion responses are shown in Fig. 14. The disturbance rejection property of the system is also verified for the case when saturation function is used shown in Fig. 16. It is observed that the effect of disturbance is negligible in the angular velocity and quaternion responses. In Figs. 15 and 17, the corresponding control torque and sliding variable responses are shown.

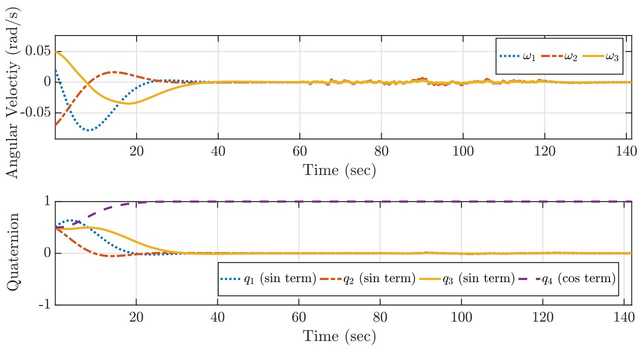

Fig. 8. Angular velocity and quaternion responses with saturation function under disturbance.

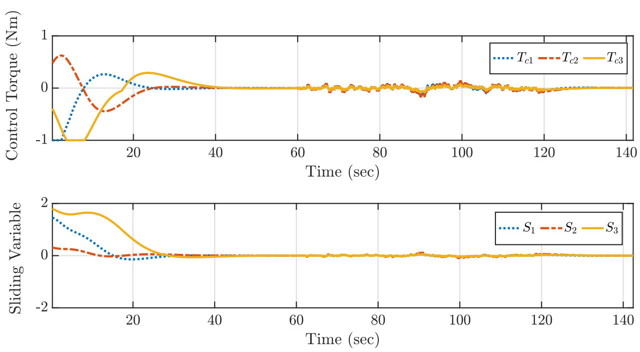

Fig. 9. Control torque and sliding variable responses with saturation function under disturbance.

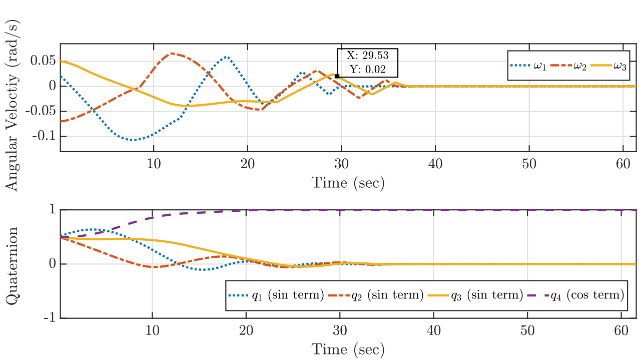

Fig. 10. Angular velocity and quaternion responses without saturation.

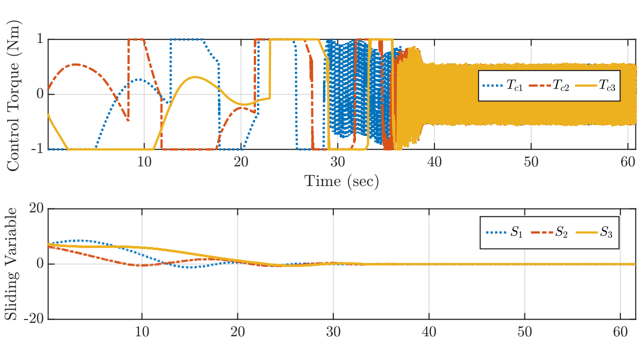

Fig. 11. Control torque and sliding variable responses without saturation.

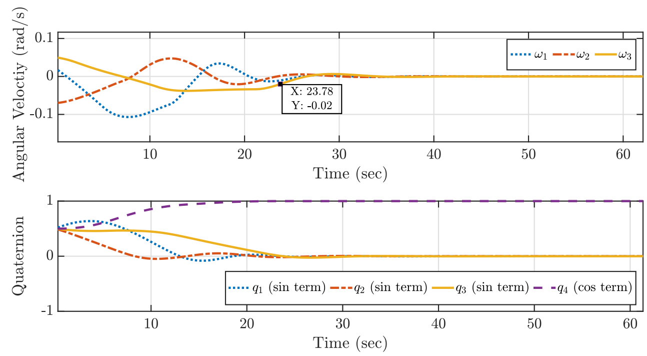

Fig. 12. Angular velocity and quaternion responses with saturation function.

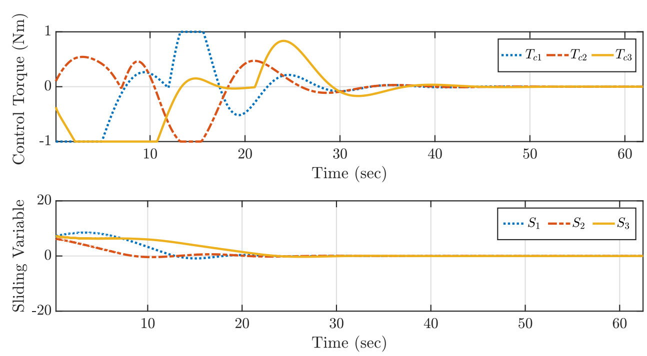

Fig. 13. Control torque and sliding variable responses with saturation function.

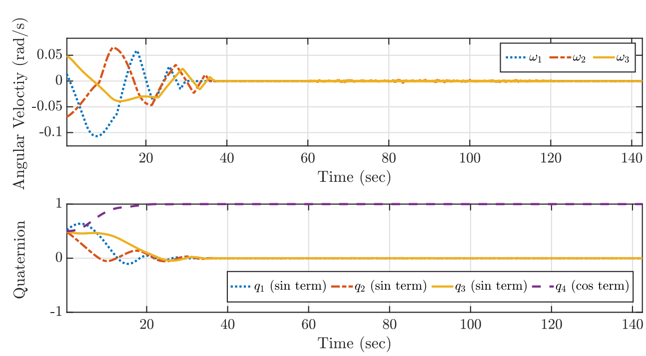

Fig. 14. Angular velocity and quaternion responses under disturbance.

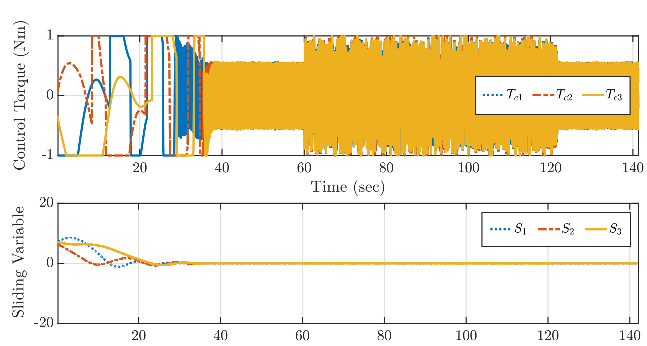

Fig. 15. Control torque and sliding variable responses under disturbance.

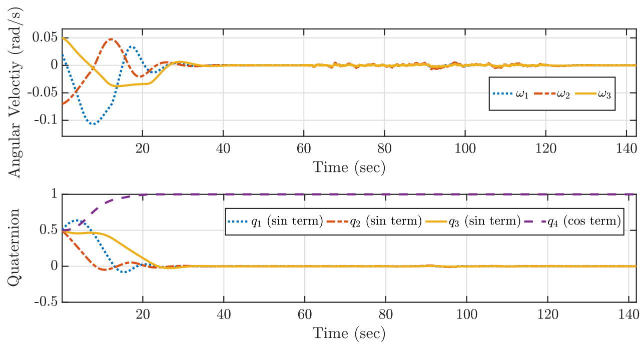

Fig. 16. Angular velocity and quaternion responses with saturation function under disturbance.

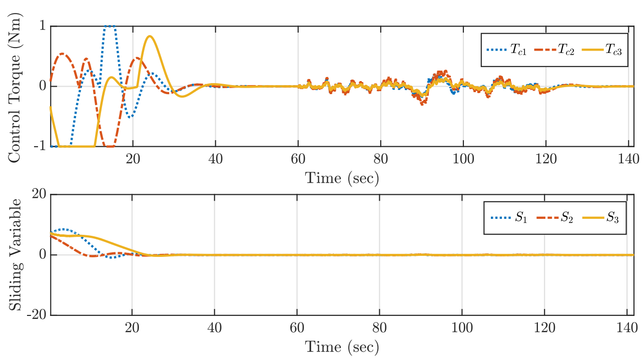

Fig. 17. Control torque and sliding variable responses with saturation function under disturbance.

4.2.2.4. Case 4: With inertia matrix perturbation. To check the robustness of PD^{β}-SMC, perturbation is introduced to the inertia matrix of the satellite system. The simulation is performed with 40% and 60% perturbations in inertia matrix at 120th sec. Since no change in response is found with respect to case 1, corresponding responses are not included.

4.2.3. Simulation results for PD-SMC with modified reaching law

4.2.3.1. Case 1: Without disturbance. The simulation results of satellite attitude control problem for *PD*-SMC with modified reaching law are shown in Figs. 18 and 19.

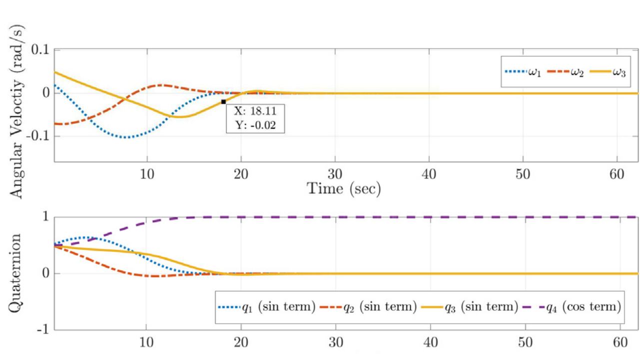

Fig. 18. Angular velocity and quaternion responses.

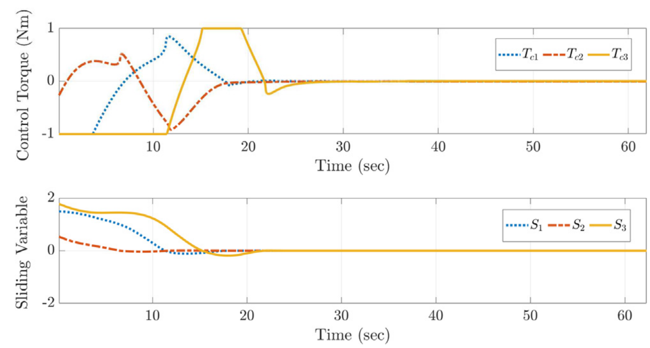

Fig. 19. Control torque and sliding variable responses.

It is observed that the desired angular velocity and quaternion settles at 18.11 s. It indicates that the settling time is considerably reduced in comparison with *PD*-SMC. It can also be noted that the chattering is completely eliminated with modified *PD*-SMC.

4.2.3.2. Case 2: With disturbance. The disturbance rejection condition in case of modified *PD*-SMC is verified by introducing a random disturbance to the system during 60th sec to 120th sec, shown in Fig. 20. The result indicates that the controller is having good disturbance rejection capability without disturbing the reaching phase of the states. Corresponding control torque and sliding variable responses are given in Fig. 21.

4.2.3.3. Case 3: With inertia matrix perturbation. The robustness of the modified *PD*-SMC is verified by perturbing the inertia matrix of the satellite at 120th sec. 40% and 60% perturbation in inertia matrix are used for simulation. It is seen that modified *PD*-SMC provides robustness against inertia uncertainty in comparision to normal condition and hence, the corresponding results are not shown.

4.2.4. Simulation results for PD^{β}-SMC with modified reaching law

4.2.4.1. Case 1: Without disturbance. Figs. 22 and 23 presents the angular velocity and quaternion responses of satellite attitude system for PD^{β}-SMC with modified reach-

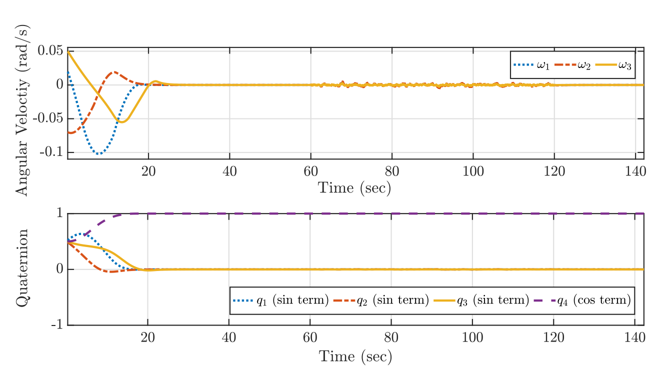

Fig. 20. Angular velocity and quaternion responses under disturbance.

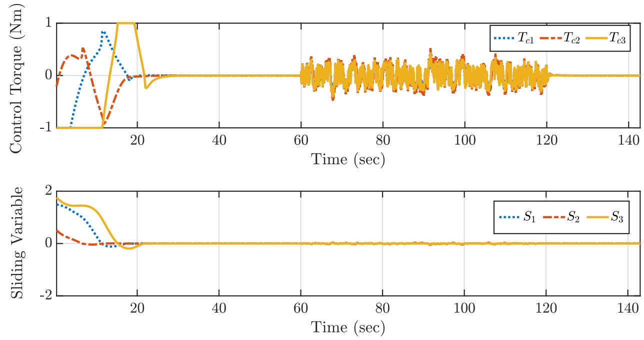

Fig. 21. Control torque and sliding variable responses under disturbance.

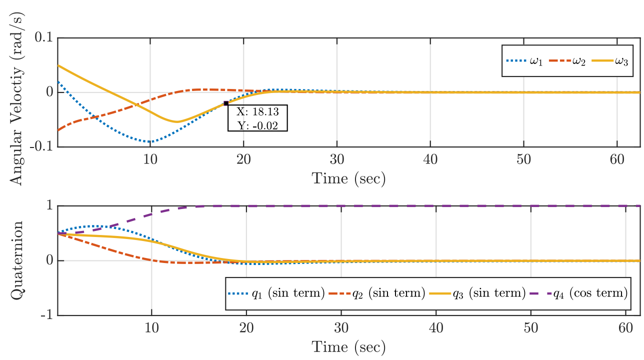

Fig. 22. Angular velocity and quaternion responses.

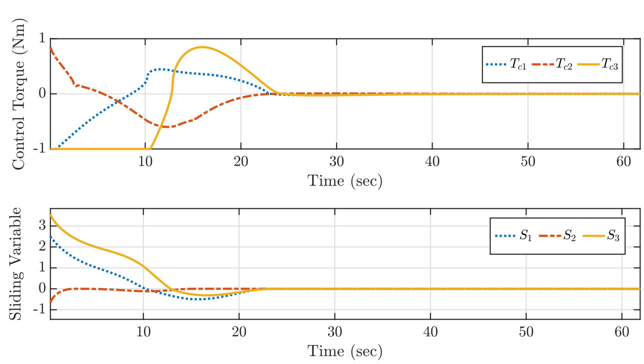

Fig. 23. Control torque and sliding variable responses.

ing law. It is noted that the response is chattering free and takes 18.13 s to settle which is less compared to PD^{β}-SMC.

4.2.4.2. Case 2: With disturbance. To show the disturbance rejection capability of the modified PD^{β}-SMC, a random disturbance is introduced to the system during 60th sec to 120th sec shown in Fig. 24. From the response, it is observed that the controller shows good disturbance rejection capability without effecting the reaching phase. The control torque and sliding variable responses are provided in Fig. 25.

4.2.4.3. Case 3: With inertia matrix perturbation. The simulation is performed with 40% and 60% perturbation in inertia matrix at 120th sec, to show the robustness of the

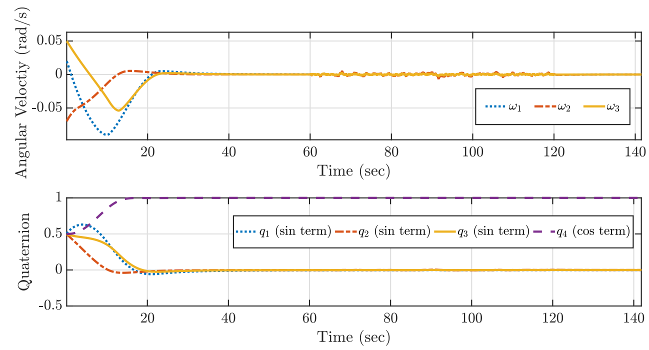

Fig. 24. Angular velocity and quaternion responses under disturbance.

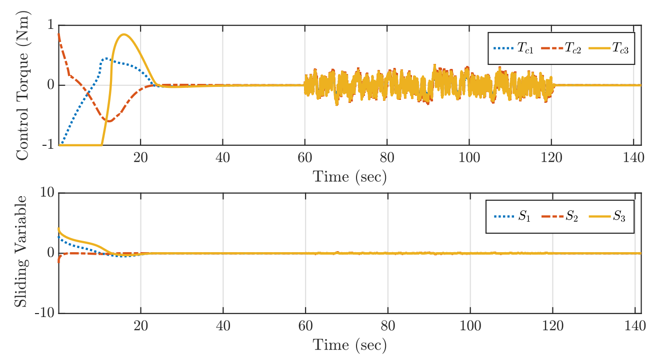

Fig. 25. Control torque and sliding variable responses under disturbance.

modified PD^{β}-SMC. It is observed that modified *PD*-SMC provides robustness against inertia uncertainty in comparision to normal condition. Since no variation is found, the corresponding responses are not shown.

4.3. Performance comparison of different controllers

To compare the control algorithms proposed in this paper, two performance indices are considered in this work namely (i) control effort and (ii) reaching time (T_{reach}) (T_{reach} indicates maximum of the reaching time towards sliding surface among all 3 axes). The performance indices of the respective controllers are computed for 200 s and are listed in Table 4.

From Table 4, it is observed that *PD*-SMC with saturation function provides least control effort in comparison to other controllers. However, the introduction of saturation function causes more reaching time compared to other controllers. This problem is addressed by introducing the modified reaching law of *PD*-SMC. The simulation results show the *PD*-SMC with modified reaching law provides less reaching time with slighlty increased control effort. Similar trend is observed for PD^{β}-SMC with/without modified reaching law.

In short, *PD*-SMC with modified reaching law provides minimum reaching time compared to other controllers. However, the control effort required is slightly higher in comparison to *PD*-SMC with saturation function and

Table 4
Performance comparision of different controllers.

Controller Name		Performance Index	
		Control Effort	Reaching Time (T_{reach}, in seconds)
PD -SMC	Without saturation function	309.7	25.779
	With saturation function	17.09	66.251
PD-SMC with modified reaching law		27.56	23.477
PD^{β}- SMC	Without saturation function	156.2	36.166
	With saturation function	30	109.092
PD^{β}-SMC with modified reaching law		22.93	29.196

PD^{β}-SMC with modified reaching law. Since PD-SMC with saturation, PD-SMC with modified reaching law and PD^{β}-SMC with saturation have either less control effort or less reaching time, PD^{β}-SMC with modified reaching law can be considered as an optimal controller for satellite attitude control system.

5. Conclusion

This paper presented the detailed study of four sliding mode satellite attitude controllers namely PD-SMC, PD^{β}-SMC, PD-SMC with modified reaching law, and PD^{β}-SMC with modified reaching law. All these control laws were developed to ensure the tracking, disturbance rejection property and robustness towards sytem parameter uncertainty. The chattering effect was present in the responses of PD-SMC and PD^{β}-SMC and it was eliminated by introducing saturation function. However, chattering was removed in cost of detoriation in robustness against disturbance as reaching time had drastically increased. The power rate type reaching law had been proposed as an alternative solution to the chattering problem. This law had been used in PD-SMC with modified reaching law and PD^{β}-SMC with modified reaching law. The simulation results show that chattering had been completely removed without effecting the robustness property. Interestingly, it was found that PD-SMC with modified reaching law provided minimum reaching time compared to other controllers. PD-SMC with saturation function provided minimum control effort in comparison to other controllers. Since optimal control effort and reaching time was essential for satellite control application, PD^{β}-SMC with modified reaching law was recommended.

The future direction of the research work is as follows: (i) to develop a new form of fractional controller so that both energy and reaching time will be minimum, (ii) although the control laws proposed in this paper shows good robustness towards parameter uncertainity, robustness can be further enhanced by applying adaptivity in the control law and (iii) the effect of disturbances like solar radiation pressure, gravity effect due to geoid shape of Earth, effect of Earth's magnetic field etc. are not considered in this work. But they have significant impact on satellite attitude in practical scenario. All these disturbances can be modelled by equations and simulated based on the real time data for validating the performance of the controllers.

Appendix A. *A.1. Proof of finite time convergence, stability and reaching time calculation for PD-SMC*

Proof of Finite Time Convergence. Finite time convergence (FTC) to the sliding surface is proved using Lyapunov function method. Followed from Tianyi et al. (2015) and Liwei and Shenmin (2013), consider the Lyapunov function as,

$$V_{PD-SMC} = \frac{1}{2K_D} S^T JS, \tag{A.1}$$

where $K_D > 0$ and J is the moment of inertia matrix (positive definite). Therefore $\frac{1}{K_D}J$ is positive definite matrix. S is the sliding surface defined in case of PD-SMC law (12).

Taking time derivative of both sides of (A.1),

$$\begin{aligned}
\dot{V}_{PD-SMC} &= \tfrac{1}{K_D} S^T J\dot{S} \\
&= \tfrac{1}{K_D} S^T J(K_P Q_e \omega_e + K_D J^{-1} \\
&\quad [T_{control} + T_d - \omega_e \times (J\omega_e + h_w)]) \\
&\quad (\text{using (3) and (17)}) \\
&= \tfrac{1}{K_D} S^T J(K_P Q_e \omega_e + K_D J^{-1}[\omega_e \times (J\omega_e + h_w) \\
&\quad -\tfrac{K_P}{K_D} J Q_e \omega_e \\
&\quad -Ksgn(S) + T_d - \omega_e \times (J\omega_e + h_w)]) (\text{using (19)}) \\
&= \tfrac{1}{K_D} S^T J(K_P Q_e \omega_e + K_D J^{-1}[-\tfrac{K_P}{K_D} J Q_e \omega_e - Ksgn(S) + T_d]) \\
&= \tfrac{1}{K_D} K_D S^T JJ^{-1}(T_d - Ksgn(S)) \\
&= -S^T(Ksgn(S) - T_d)
\end{aligned} \tag{A.2}$$

If K is positive scalar such that $K \geqslant \|T_d\|_\infty$, then from (A.2),

$$\begin{aligned}
&\dot{V}_{PD-SMC} \leqslant -\|S\|_1 (\eta \text{ reachability condition}) \\
\Rightarrow\ &\dot{V}_{PD-SMC} \leqslant -\|S\|_2 \\
\Rightarrow\ &\dot{V}_{PD-SMC} \leqslant -\sqrt{\tfrac{2K_D}{\lambda_{max}(J)}} V^{\frac{1}{2}}_{PD-SMC} \ (\text{from(A.11)})
\end{aligned} \tag{A.3}$$

where λ_{max} is the maximum eigen value of J. Also, let $\eta = \sqrt{\frac{2K_D}{\lambda_{max}(J)}}$.

Then (A.3) gives,

$$\dot{V}_{PD-SMC} + \eta V_{PD-SMC}^{\frac{1}{2}} \leqslant 0$$

Since the function $\dot{V}_{PD-SMC} + \eta V_{PD-SMC}^{\frac{1}{2}}$ is negative semi-definite. From Lemma 1 of Tianyi et al. (2015), it shows that the system reaches sliding surface in finite time. Therefore, FTC of the system is proved.

Proof of Stability. Consider the surface S in (12). At $t = t_{reach}, S = 0$. This implies,

$$\begin{aligned} & 2K_P q_e + K_D \omega_e = 0 \\ \Rightarrow \quad & \omega_e = -2\tfrac{K_P}{K_D} q_e \end{aligned} \tag{A.5}$$

To ensure the stability, the Lyapunov function candidate is chosen as Yu et al. (2011),

$$V_q = \frac{1}{2} q_e^T q_e \tag{A.6}$$

Differentiating (A.6) with respect to time and it follows as,

$$\begin{aligned} \dot{V}_q = & \; q_e^T \dot{q}_e \\ = & \; \tfrac{1}{2} q_e^T Q_e \omega_e (\text{using (16)}) \\ = & \; \tfrac{1}{2} q_e^T Q_e.(-2\tfrac{K_P}{K_D}) q_e (\text{using (A.5)}) \\ = & \; -\tfrac{K_P}{K_D} q_e^T Q_e q_e \\ = & \; -\tfrac{K_P}{K_D} q_{e4} \|q_e\|^2 \end{aligned} \tag{A.7}$$

Under the condition $K_P > 0, K_D > 0$, and also considering $q_{e4} > 0$ always, we have $\dot{V}_q <= 0$. Hence V_q satisfies the following conditions:

1. $V_q > 0$ if $q_e \neq 0$
2. $V_q = 0$ if $q_e = 0$
3. $\dot{V}_q <= 0, \dot{V}_q$=0 if and only if $q_e = [0, 0, 0]^T$

By using Lyapunov Theorem Strogatz (2018), $q_e = [0, 0, 0]^T$ is asymptotically stable and $q_e \rightarrow [0, 0, 0]^T$ is guaranteed.

Calculation of Reaching Time: Let us denote V_{PD-SMC} at $t = 0$ by $V_1(S_0)$. Considering that V_{PD-SMC} becomes zero after reaching the sliding surface, integrating both sides of (A.4) in the time limit from 0 to t_{reach} (reaching time),

$$t_{reach} \leqslant \frac{2}{\eta} \sqrt{V_1(S_0)} \tag{A.8}$$

Hence, expression for maximum reaching time is given by,

$$t_{reach}|_{max} = \frac{2}{\eta} \sqrt{V_1(S_0)} \tag{A.9}$$

Putting value of η in (A.9),

$$t_{reach}|_{max} = \sqrt{\frac{2}{K_D} \lambda_{max}(J) V_1(S_0)} \tag{A.10}$$

A.2. Proof of finite time convergence, stability & reaching time calculation for $PD^\beta - SMC$

Proof of Finite Time Convergence. In this case, Lyapunov function used is chosen same as in (A.1),

$$V_{PD^\beta-SMC} = \frac{1}{2K_D} S^T J S \tag{A.11}$$

where S is the sliding surface for PD^β-SMC law as described by (20).

Differentiating $V_{PD^\beta-SMC}$ with respect to time,

$$\begin{aligned} \dot{V}_{PD^\beta-SMC} = & \; \tfrac{1}{K_D} S^T J \dot{S} \\ = & \; \tfrac{1}{K_D} S^T J (K_P Q_e \omega_e + K_D D^\beta J^{-1} \\ & [T_{control} + T_d - \omega_e \times (J\omega_e + h_w)]) \\ & (\text{using (3) and (20)}) \\ = & \; \tfrac{1}{K_D} S^T J (K_P Q_e \omega_e + K_D D^\beta J^{-1} \\ & [\omega_e \times (J\omega_e + h_w)] - \tfrac{K_P}{K_D} J D^{-\beta} Q_e \omega_e \\ & -K_f D^{-\beta} sgn(S) + T_d - \omega_e \times (J\omega_e + h_w)]) \\ & (\text{using (25)}) \\ = & \; \tfrac{1}{K_D} S^T J (K_P Q_e \omega_e + K_D D^\beta J^{-1} \\ & [-\tfrac{K_P}{K_D} J D^{-\beta} Q_e \omega_e - K_f D^{-\beta} sgn(S) + T_d]) \\ = & \; \tfrac{1}{K_D} K_D S^T J J^{-1} D^\beta (T_d - K_f D^{-\beta} sgn(S)) \end{aligned}$$

$$\Rightarrow \dot{V}_{PD^\beta-SMC} = -S^T (K_f sgn(S) - D^\beta T_d) \tag{A.12}$$

If K_f is positive scalar such that $K_f \geqslant \|D^\beta T_d\|_\infty$. Then from (A.12),

$$\begin{aligned} & \dot{V}_{PD^\beta-SMC} \leqslant -\|S\|_1 \\ \Rightarrow \quad & \dot{V}_{PD^\beta-SMC} \leqslant -\|S\|_2 \\ \Rightarrow \quad & \dot{V}_{PD^\beta-SMC} \leqslant -\sqrt{\tfrac{2K_D}{\lambda_{max}(J)}} V_{PD^\beta-SMC}^{\frac{1}{2}} (\text{using(A.11)}) \end{aligned} \tag{A.13}$$

Let, $\eta_f = \sqrt{\frac{2K_D}{\lambda_{max}(J)}}$ then (A.13) simplifies to,

$$\dot{V}_{PD^\beta-SMC} + \eta_f V_{PD^\beta-SMC}^{\frac{1}{2}} \leqslant 0$$

From (A.14), FTC is confirmed when PD^β-SMC control law is used Tianyi et al. (2015).

Proof of Stability. From (20) we get,

$$\begin{aligned} & 2K_P q_e + K_D D^\beta \omega_e = 0 \\ \Rightarrow \quad & \omega_e = -\tfrac{2K_P}{K_D} D^{-\beta} q_e \\ \Rightarrow \quad & \omega_e = -\tfrac{2K_P}{K_D} \tfrac{1}{\Gamma(\beta)} \int_0^t (t-\tau)^{\beta-1} q_e(\tau) d\tau \end{aligned} \tag{A.15}$$

Considering the inequality $q_e(t) \geqslant q_e(0)$ into account (A.15) can be further simplified as,

$$\begin{aligned} & \omega_e \leqslant -\tfrac{2K_P q_e(0)}{K_D \Gamma(\beta)} \int_0^t (t-\tau)^{\beta-1} d\tau \\ & \Rightarrow \omega_e \leqslant -\tfrac{2K_P q_e(0)}{K_D \Gamma(\beta)} \tfrac{t^\beta}{\beta} \end{aligned} \tag{A.16}$$

Consider Lyapunov function be,

$$V_{qfrac} = \frac{1}{2} q_e^T q_e \tag{A.17}$$

Applying fractional derivative operator D^β on both sides of (A.17),

$$\begin{aligned} D^\beta V_{qfrac} &= D^{\beta-1}(q_e^T \dot{q}_e) \\ &= \tfrac{1}{2} D^{\beta-1}(q_e^T Q_e \omega_e)(\text{using } 16) \\ &\leqslant -\tfrac{K_P}{K_D \beta \Gamma(\beta)} D^{\beta-1}(q_e^T Q_e q_e(0) t^\beta)(\text{using (A.16)}) \end{aligned} \tag{A.18}$$

Consider the following inequality condition,

$$q_e^T Q_e q_e(0) \leqslant q_{e4}(0) \|q_e(0)\|^2 \tag{A.19}$$

Also, consider the following property of fractional derivative,

$$D^\alpha (x-a)^\gamma = \frac{\Gamma(1+\gamma)}{\Gamma(1+\gamma-1)} (x-a)^{\gamma-\alpha} \tag{A.20}$$

where x is the variable and a is constant. Substitute $\alpha = \beta - 1, \gamma = \beta, a = 0$ and replace x by t in (A.20),

$$\begin{aligned} & D^{\beta-1}(t)^\beta = \tfrac{\Gamma(1+\beta)}{\Gamma(\beta)} t \\ \Rightarrow \quad & D^{\beta-1}(t)^\beta = (\beta+1)t \end{aligned} \tag{A.21}$$

Using (A.19) and (A.21) in (A.18), it follows,

$$\begin{aligned} D^\beta V_{qfrac} \leqslant & -\tfrac{K_P}{K_D \ \beta \Gamma(\beta)} D^{\beta-1}(q_{e4}(0) \|q_e(0)\|^2 t^\beta)) \\ \leqslant & -\tfrac{K_P \ q_{e4}(0) \|q_e(0)\|^2}{K_D \ \beta \Gamma(\beta)} D^{\beta-1}(t^\beta)) \\ \leqslant & -\tfrac{K_P \ q_{e4}(0) \|q_e(0)\|^2}{K_D \ \beta \Gamma(\beta)} (\beta+1)t \end{aligned} \tag{A.22}$$

Therefore, by considering $q_{e4} > 0$,

$$D^\beta V_{qfrac} \leqslant 0$$

Hence, V_{qfrac} satisfies the following:

1. V_{qfrac} is continuously differentiable and satisfies Liptschitz's condition locally such that, $V_{qfrac} \leqslant \|q_e\|$ ($\|.\|$ means $\|.\|_1$)
2. $D^\beta V_{qfrac} \leqslant 0$ with $0 < \beta < 1$

By using Theorem in Sara et al. (2017), $q_e = [0,0,0]^T$ is asymptotically stable for any $\|q_e(0)\| < 1$. Hence q_e asymptotically converges to $[0,0,0]^T$.

Calculation of Reaching Time: Let us denote the Lyapuonv function $V_{PD^\beta - SMC}$ at $t=0$ by $V_2(S_0)$. Applying integration in both sides of (A.14) in the limit 0 to t_{reach},

$$t_{reach} \leqslant \frac{2}{\eta_f} \sqrt{V_2(S_0)} \tag{A.24}$$

Therefore, the expression for maximum reaching time is given by,

$$t_{reach}|_{max} = \frac{2}{\eta_f} \sqrt{V_2(S_0)} \tag{A.25}$$

Substituting the value of η_f in (A.25),

$$t_{reach}|_{max} = \sqrt{\frac{2}{K_D} (\lambda_{max}(J)) V_2(S_0)} \tag{A.26}$$

A.3. Proof of finite time convergence, stability & reaching time calculation for PD – SMC with modified reaching law

Proof of Finite Time Convergence. For this proof, Lyapunov function is chosen as Liwei and Shenmin (2013),

$$V_{mod} = \frac{1}{2} S^T S \tag{A.27}$$

where S being the sliding surface used for *PD*-SMC law with modified reaching law (12). From (A.27),

$$\begin{aligned} & \dot{V}_{mod} = S^T \dot{S} \\ \Rightarrow \quad & \dot{V}_{mod} = S^T(-K_m |S|^\alpha sgn(S))(\text{using}(26)) \end{aligned} \tag{A.28}$$

IF $K_m > 0$, then the diagonal matrix $K_m |S|^\alpha$ is a positive definite. Hence, by using the properties of quadratic function in (A.28),

$$\begin{aligned} & \dot{V}_{mod} \leqslant -\|S\|_1 \\ \Rightarrow \quad & \dot{V}_{mod} \leqslant -\|S\|_2 \\ \Rightarrow \quad & \dot{V}_{mod} \leqslant -\sqrt{2} V_{mod}^{\frac{1}{2}}(\text{using(A.27)}) \end{aligned} \tag{A.29}$$

Therefore,

$$\dot{V}_{mod} + \sqrt{2} V_{mod}^{\frac{1}{2}} \leqslant 0 \tag{A.30}$$

From FTC lemma Tianyi et al. (2015), it is inferred that sliding surface is achieved in finite time.

Proof of Stability. For the stability proof, same steps need to be followed as discussed in previous case (*PD*-SMC), hence the proof is not discussed here.

Calculation of Reaching Time: Let V_{mod} at $t=0$ be $V_3(S_0)$. Integration of both sides of (A.30) in the limit 0 to t_{reach} gives,

$$t_{reach} \leqslant \sqrt{2V_3(S_0)} \tag{A.31}$$

Hence, the expression for maximum reaching time is given by,

$$t_{reach}|_{max} = \sqrt{2V_3(S_0)} \tag{A.32}$$

A.4. Proof of finite time convergence, stability & reaching time calculation for PD^β – SMC with modified reaching law

Proof of Finite Time Convergence. To prove FTC, Lyapunov function chosen as,

$$V_{frac-mod} = \frac{1}{2}S^T S \tag{A.33}$$

where S is the sliding surface designed for PD^β-SMC law (20). Following the same steps for proving FTC, apply differentiation on $V_{frac-mod}$ w.r.t time and it follows as,

$$\begin{aligned} &\dot{V}_{frac-mod} = S^T\dot{S} \\ \Rightarrow \quad &\dot{V}_{frac-mod} = S^T(-K_{mf}|S|^\alpha sgn(S))(\text{from}(28)) \end{aligned} \tag{A.34}$$

$K_{mf}|S|^\alpha$ is a positive definite diagonal matrix if $K_{mf} > 0$. Hence from (A.34), using quadratic function properties,

$$\begin{aligned} &\dot{V}_{frac-mod} \leqslant -\|S\|_1 \\ \Rightarrow \quad &\dot{V}_{frac-mod} \leqslant -\|S\|_2 \\ \Rightarrow \quad &\dot{V}_{frac-mod} \leqslant -\sqrt{2}V_{frac-mod}^{\frac{1}{2}}(\text{using}(A.33)) \end{aligned} \tag{A.35}$$

Therefore,

$$\dot{V}_{frac-mod} + \sqrt{2}V_{frac-mod}^{\frac{1}{2}} \leqslant 0 \tag{A.36}$$

By using Lemma 1 of Tianyi et al. (2015), FTC is proved.

Proof of Stability. Since the sliding surface for this control law is same as in (20), the stability proof is not presented.

Calculation of Reaching Time: Consider the Lyapunov function $V_{frac-mod}$ at $t = 0$ be denoted by $V_4(S_0)$. Expression for reaching time is obtained by integrating both sides of (A.36) in the limit 0 to t_{reach} and is given by,

$$t_{reach} \leqslant \sqrt{2V_4(S_0)} \tag{A.37}$$

Hence, the maximum reaching time expression is obtained as,

$$t_{reach}|_{max} = \sqrt{2V_4(S_0)} \tag{A.38}$$

Appendix B. Mathematical modelling of inertia matrix perturbation and disturbance torque condition and their effect on the attitude model of satellite

- **Modelling of Inertia Matrix Perturbation:**Consider, J_0 be the nominal value of the satellite inertia matrix and Δx be the amount of perturbation. Then the perturbed inertia matrix of the satellite is given by,

$$J = (1 + \Delta x)J_0 \tag{B.1}$$

where, Δx is applied on each element of diagonal matrix J_0. In this paper, inertia matrix perturbed by 40% and 60% at $t = 120$ sec. Therefore the values of Δx for the two cases are 0.4 and 0.6 respectively. From Table 1, the nominal inertia matrix (J_0) of the satellite is,

$$J_0 = diag[50, 75, 100] \text{ Kg m}^2 \tag{B.2}$$

Therefore, the satellite inertia matrix perturbation condition can be formulated as,

$$J(t) = \begin{cases} J_0 & t < 120 \text{ sec} \\ (1 + \Delta x)J_0 & t \geqslant 120 \text{ sec} \end{cases} \tag{B.3}$$

- **Modelling of Disturbance Torque:**The disturbance torque is applied to the system during 60th sec to 120th sec. The disturbance torque considered in this work, is uniform random type, whose expression is as following:

$$T_d = \begin{bmatrix} rand(-5, 5) \\ rand(-12, 12) \\ rand(-7, 7) \end{bmatrix} (\text{in N m}) \tag{B.4}$$

where $rand(a, b)$ provides a uniform random number in the range $[a, b]$.

Hence, the disturbance torque condition is given by,

$$T_d(t) = \begin{cases} \begin{bmatrix} rand(-5, 5) \\ rand(-12, 12) \\ rand(-7, 7) \end{bmatrix} & 60 \text{ sec} \leqslant t \leqslant 120 \text{ sec} \\ 0_{3\times1} & \text{otherwise} \end{cases} \tag{B.5}$$

Therefore, the overall nonlinear model of the satellite's angular motion (from Eqn. (9)) considering the inertia matrix perturbation and disturbance torque condition is as below,

$$\frac{d}{dt}\begin{bmatrix} \omega \\ q \\ q_4 \\ h_w \\ \dot{h}_w \end{bmatrix} = \begin{bmatrix} J^{-1}(-\omega \times (J\omega + h_w) + T_c + T_d) \\ -\frac{1}{2}\omega \times q + \frac{1}{2}q_4 I_{3\times3}\omega \\ -\frac{1}{2}\omega^T q \\ -T_c \\ -\frac{1}{\tau_w}\dot{h}_w + \frac{1}{\tau_w}T_w \end{bmatrix} \tag{B.6}$$

where, $J \equiv J(t)$ and $T_d \equiv T_d(t)$ are followed from Eqn. (B.3) and Eq. (B.5) respectively.

References

Abdulhamitbilal, E., Jafarov, E.M., 2006. Performances comparison of linear and sliding mode attitude controllers for flexible spacecraft with reaction wheels. In: International Workshop on Variable Structure Systems, 2006. VSS'06., pp. 351–358.

Abdulhamitbilal, E., Jafarov, E.M., 2008. Sliding mode attitude controller design for nonlinear flexible geosynchronous satellite with thrust jets. In: 2008 International Workshop on Variable Structure Systems, pp. 221–226.

Abdulhamitbilal, E., Jafarov, E.M., 2012. Design of Sliding Mode Attitude Control for Communication Spacecraft. INTECH Open Access Publisher.

Acob, J.M., Pano, V., Ouyang, P.R., 2013. Hybrid pd sliding mode control of a two degree-of-freedom parallel robotic manipulator. In: 2013 10th IEEE International Conference on Control and Automation (ICCA). IEEE, pp. 1760–1765.

Ahmed, R., Kardous, Z., Braie, K.N.B., 2012. A pid sliding mode control design for a coupled tank. In: International Conference CRATT, pp. 1–6.

Ahmed, S., Wang, H., Tian, Y., 2018. Model-free control using time delay estimation and fractional-order nonsingular fast terminal sliding mode for uncertain lower-limb exoskeleton. J. Vib. Control 24, 5273–5290.

Ahmed, S., Wang, H., Tian, Y., 2019a. Adaptive high-order terminal sliding mode control based on time delay estimation for the robotic manipulators with backlash hysteresis. IEEE Trans. Syst. Man Cybernet.: Syst.

Ahmed, S., Wang, H., Tian, Y., 2019b. Robust adaptive fractional-order terminal sliding mode control for lower-limb exoskeleton. Asian J. Control 21, 473–482.

Bandyopadhyay, B., Janardhanan, S., Spurgeon, S.K., 2013. Advances in sliding mode control. Lecture Notes in Control and Information Sciences, LNCiS Springer 440.

Bekir, E., 2007. Introduction to Modern Navigation Systems. World Scientific.

Blanke, M., Larsen, M.B., 2010. Satellite dynamics and control in a quaternion formulation. Technical Report. Technical University of Denmark, Department of Electrical Engineering.

Bryson Jr, A.E., 2015. Control of Spacecraft and Aircraft. Princeton University Press.

Chen, Y.P., Lo, S.C., 1993. Sliding-mode controller design for spacecraft attitude tracking maneuvers. In: 1993 American Control Conference, pp. 195–196.

Chen, Z., Cong, B., Liu, X., 2013. Robust control of spacecraft eigenaxis maneuver via integral sliding mode. In: 2013 25th Chinese Control and Decision Conference (CCDC), pp. 1758–1763.

Crassidis, J.L., Markley, F.L., 1996. Sliding mode control using modified rodrigues parameters. J. Guid. Control Dyn. 19, 1381–1383.

Devika, K., Thomas, S., 2017. Improved sliding mode controller performance through power rate exponential reaching law. In: 2017 Second International Conference on Electrical, Computer and Communication Technologies (ICECCT). IEEE, pp. 1–7.

Edwards, C., Spurgeon, S., 1998. Sliding Mode Control: Theory and Applications. Crc Press.

Eker, I., 2006. Sliding mode control with pid sliding surface and experimental application to an electromechanical plant. ISA Trans. 45, 109–118.

Froelich, R., Papapoff, H., 1959. Reaction wheel attitude control for space vehicles. IRE Trans. Automatic Control 4, 139–149.

Gao, W., Hung, J.C., 1993. Variable structure control of nonlinear systems: a new approach. IEEE Trans. Industr. Electron. 40, 45–55.

Ghazali, R., Sam, Y.M., Rahmat, M.F., Hashim, A.W.I.M., et al., 2011. Performance comparison between sliding mode control with pid sliding surface and pid controller for an electro-hydraulic positioning system. Int. J. Adv. Sci. Eng. Inf. Technol. 1, 447–452.

Ibrahim, A.E., Tobal, A.M., Sultan, M.A., 2012. Satellite attitude maneuver using sliding mode control under body angular velocity constraints. Int. J. Comput. Appl. 50.

Jerouane, M., Sepehri, N., Lamnabhi-Lagarrigue, F., 2004. Dynamic analysis of variable structure force control of hydraulic actuators via the reaching law approach. Int. J. Control 77, 1260–1268.

Jin, S., Bak, J., Kim, J., Seo, T., Kim, H.S., 2018. Switching pd-based sliding mode control for hovering of a tilting-thruster underwater robot. PloS One 13, e0194427.

Kailil, A., Mrani, N., Abid, M., Choukri, S., Touati MLIHA, M., Elalami, N., 2004a. Fractional regulators for spacecraft attitude stabilization. In: 22nd AIAA International Communications Satellite Systems Conference & Exhibit 2004 (ICSSC), p. 3117.

Kailil, A., Mrani, N., Mliha Touati, M., Choukri, S., Elalami, N., 2004b. Low earth-orbit satellite attitude stabilization with fractional regulators. Int. J. Syst. Sci. 35, 559–568.

Kang, J., Zhu, Z.H., Wang, W., Li, A., Wang, C., 2017. Fractional order sliding mode control for tethered satellite deployment with disturbances. Adv. Space Res. 59, 263–273.

Kuipers, J.B. et al., 1999. Quaternions and Rotation Sequences, vol. 66. Princeton University Press, Princeton.

Lazarević, M., 2012. Fractional order control of a robot system driven by dc motors. Sci. Tech. Rev. ISSN 206, 20–29.

Liu, J., Wang, X., 2012. Advanced Sliding Mode Control for Mechanical Systems: Design, Analysis and MATLAB Simulation. Springer Science & Business Media.

Liwei, D., Shenmin, S., 2013. Attitude control of pico-satellite using flywheel based on fractional order sliding mode. In: Proceedings of 2013 2nd International Conference on Measurement, Information and Control, pp. 756–761.

Lu, K., Xia, Y., Zhu, Z., Basin, M.V., 2012. Sliding mode attitude tracking of rigid spacecraft with disturbances. J. Franklin Inst. 349, 413–440.

Mirhassani, S.M., Ahmadian, J., Ghorbanian, M.J., Hassan, M.A., 2013. Stability of geostationary flying satellite under combined sliding mode and pid control. In: 2013 IEEE Business Engineering and Industrial Applications Colloquium (BEIAC), pp. 115–119.

Monje, C.A., Chen, Y., Vinagre, B.M., Xue, D., Feliu-Batlle, V., 2010. Fractional-order Systems and Controls: Fundamentals and Applications. Springer Science & Business Media.

Ouyang, P., Acob, J., Pano, V., 2014. Pd with sliding mode control for trajectory tracking of robotic system. Robot. Comput.-Integrated Manuf. 30, 189–200.

Qi, T., Wang, H., 2016. Pid sliding mode controller design and application to active queue management. In: 2016 35th Chinese Control Conference (CCC). IEEE, pp. 6917–6922.

Rahimian, M.A., Tavazoei, M.S., 2013. Optimal tuning for fractional-order controllers: an integer-order approximating filter approach. J. Dyn. Syst. Meas. Contr. 135, 021017.

Sara, Dadras, S., Malek, H., Chen, Y., 2017. A note on the lyapunov stability of fractional-order nonlinear systems. In: ASME 2017 International Design Engineering Technical Conferences and Computers and Information in Engineering Conference, American Society of Mechanical Engineers. pp. V009T07A033–V009T07A033.

Shtessel, Y., Edwards, C., Fridman, L., Levant, A., 2014. Sliding Mode Control and Observation. Springer.

Siahpush, A., Gleave, J., 1988. A brief survey of attitude control systems for small satellites using momentum concepts.

Sidi, M.J., 1997. 'Spacecraft dynamics and control: a practical engineering approach., vol. 7. Cambridge University Press.

Song, Y., Liu, Z., Ouyang, H., Wang, H., Lu, X., 2017. Sliding mode control with pd sliding surface for high-speed railway pantograph-catenary contact force under strong stochastic wind field. Shock Vib. 2017.

Strogatz, S.H., 2018. Nonlinear Dynamics and Chaos with Student Solutions Manual: With Applications to Physics, Biology, Chemistry, and Engineering. CRC Press.

Tang, J., Ouyang, P.R., Yue, W., Kang, H., 2017. Nonlinear pd sliding mode control for robotic manipulator. In: 2017 IEEE International Conference on Advanced Intelligent Mechatronics (AIM). IEEE, pp. 1004–1008.

Tepljakov, A., Petlenkov, E., Belikov, J., 2011. Fomcon: Fractional-order modeling and control toolbox for matlab. In: Proceedings of the 18th International Conference Mixed Design of Integrated Circuits and Systems – MIXDES 2011, pp. 684–689.

Tianyi, Z., Xuemei, R., Yao, Z., 2015. A fractional order sliding mode controller design for spacecraft attitude control system. In: 2015 34th Chinese Control Conference (CCC), pp. 3379–3382.

Utkin, V.I., 1993. Sliding mode control design principles and applications to electric drives. IEEE Trans. Industr. Electron. 40, 23–36.

Vadali, S., 1986. Variable-structure control of spacecraft large-angle maneuvers. J. Guid. Control Dyn. 9, 235–239.

Valério, D., 2012. Introducing fractional sliding mode control. Proceedings of The Encontro de Jovens Investigadores do LAETA FEUP, 2012.

Wertz, J.R., 2012. Spacecraft attitude determination and control., vol. 73. Springer Science & Business Media.

Wie, B., 1998. Space vehicle dynamics and control. Aiaa.

Wu, S., Sun, Z., Li, H., 2009. Sliding mode controller design for rigid satellite attitude tracking. In: 2009 IEEE International Conference on Robotics and Biomimetics (ROBIO). IEEE, pp. 2238–2243.

Xinsheng, W., Huaqiang, Z., 2015. Fractional order controller for satellite attitude control system with pwpf modulator. In: 2015 34th Chinese Control Conference (CCC). IEEE, pp. 5758–5763.

Xue, D., Chen, Y., Atherton, D.P., 2007. Linear feedback control: analysis and design with MATLAB. SIAM.

Young, K.D., Utkin, V.I., Ozguner, U., 1996. A control engineer's guide to sliding mode control. In: Proceedings. 1996 IEEE International Workshop on Variable Structure Systems.-VSS'96-, IEEE. pp. 1–14.

Yu, P., Xia, K., Li, J., 2011. A design of reconfigurable satellite control system with reaction wheels based on error quaternion model. In: 2011 International Conference on Internet Computing and Information Services. IEEE, pp. 215–218.